Superconducting Gaps via Raman Scattering in Iron Superconductors

Chandan Setty[1] and Jiangping Hu[2, 1, 3]

[1] *Department of Physics and Astronomy, Purdue University, West Lafayette, Indiana 47907, USA*
[2] *Beijing National Laboratory for Condensed Matter Physics, Institute of Physics, Chinese Academy of Sciences, Beijing 100080, China*
[3] *Collaborative Innovation Center of Quantum Matter, Beijing, China*

We investigate non-resonant Raman response for iron-based superconductors using the framework of an effective S_4 model that was recently proposed to capture the essential electronic and magnetic properties of Iron based superconductors. We compute the momentum matrix elements and the resulting Raman vertices exactly for different polarization geometries and amazingly find that a simple $cosk_x cosk_y$ superconducting gap function is in good agreement with experimental data measured in both iron-pnictides and iron-chalcogenides. The Raman peaks are also matched quantitatively with the measured superconducting gaps by other experimental techniques. The result strengthens the validity of the S_4 model and the dominance of the s-wave pairing for iron-based superconductors.

arXiv:1404.7745v1 [cond-mat.supr-con] 30 Apr 2014

The discovery of Iron based superconductors [1, 2] has inspired continued searches for new ways of understanding the mechanism of superconductivity. The major difficulty in understanding their electronic structure is the occurrence of multiple bands at the Fermi level. Although many effective model Hamiltonians - constructed by including different number of orbitals like two[3], three[4] and five [5] orbitals - have been proposed, their successes are limited; that is, while simple two and three orbital models leave out several essential features observed in experiments, five orbital models lack analytical and numerical tractability which makes it hard for theoretical calculations to predict meaningful results and therefore, fail to isolate the vital ingredients which control the diverse and interesting phenomena observed in experiments.

Recently it was suggested that the underlying, low energy, electronic structure in the iron based superconductors was governed by an S_4 symmetric, two weakly coupled, single orbital models [6]. The motivation for such a model, henceforth referred to as the S_4 model, was derived from the fact that if the hopping parameters in the original five band model [5] are tranformed to a different gauge setting, then, one can use the effective d_{xz} and d_{yz} orbitals to construct a model that accurately describes the essential band structure near Fermi levels. In the real space picture, the two orbitals can be naturally segmented into two groups : one, coupled to the As atoms on the top of the Fe layer and the other, to those at the bottom, with each group containing contributions from both the sub-lattices. It was also demonstrated that the gauge transformation maps the $s-$wave pairing symmetry in the original one Fe Brillouin Zone (BZ) to the $d-$ wave pairing symmetry in the folded BZ defined on the two sublattices, thus establishing that the relevant symmetry which unifies the different families of high T_c superconductors is a combination of both the hopping and the pairing symmetries. It remains, now, to compute the consequences and predictions of such a model, examine its accuracy, and determine its suitability in describing the observed experimental phenomena. It is important to note that the critical difference between the S_4 model and the previous 2-orbital model[3] is that the latter fails in capturing the band dispersions of the hole pockets at Γ and the electron pockets at M.

Electronic Raman scattering in superconductors [7–9] has proved to be a powerful tool for determining the structure and symmetry of the superconducting gap. The Raman scattering vertex, in general, can have contributions from all the irreducible representations (irreps) of the point group of the crystal; however, a proper choice of the polarization geometries of the incoming and outgoing light beams can single out contributions from a single irrep to the total scattering cross section. As a result of the weighted BZ averaging, the quasiparticle energy gaps are probed only in selected directions in the BZ depending on the symmetry of chosen irrep and can, therefore, give information about the different types of anisotropies in the superconducting gap. The spectral features in different scattering geometries, pairing symmetries, peak positions, anisotropies, low frequency and temperature behavior, coulomb screening effects and final state interactions have all been taken into account in evaluating the response functions for both the cuprates [7, 9] and the pnictides [10–12].

In this letter, we evaluate the non-resonant Raman response of the hole/electron doped 122 pnictide and electron overdoped 122 chalcogenide by computing the momentum matrix elements and the resulting Raman vertices exactly (within the tight binding approximation) for different polarization geometries. Here, we amazingly find that using a simple $cosk_x cosk_y$ form of the gap function with a combination of the vertices and certain other properties of the S_4 model, one can successfully account for the Raman data reported in [13, 14]. In this case, the Raman peaks are even consistently matched

with the quantitative values of the superconducting gaps measured by Angle Resolved Photoemission Spectra (ARPES) experiments in these materials. The result strengthens the validility of this simplest model and the dominance of the s-wave pairing in both iron-pnictides and iron-chalcogenides.

The scattered light intensity in a Raman experiment is written in terms of the differential photon scattering cross section as

$$\frac{\partial^2\sigma}{\partial\omega\partial\Omega} = \frac{\omega_S}{\omega_I} r_0^2 S_{\gamma\gamma}(\mathbf{q},\omega) \tag{1}$$

$$S_{\gamma\gamma}(\mathbf{q},\omega) = -\frac{1}{\pi}[1+n(\omega)] Im\chi_{\gamma\gamma}(\mathbf{q},\omega), \tag{2}$$

where ω_I and ω_S are the frequencies of the incident and scattered photons respectively and $r_0 = \frac{e^2}{mc^2}$ is the Thompson radius. The imaginary part of the Raman response function is related to the generalized structure factor $S_{\gamma\gamma}$ through the fluctuation-dissipation theorem (eq. 2) and $n(\omega)$ is the Bose-Einstein distribution function. The long wavelength Raman reponse measures effective 'anisotropic' density fluctuations

$$\chi_{\gamma\gamma}(\omega) = \int_0^\beta d\tau e^{-i\omega_m\tau} \langle T_\tau \tilde{\rho_\gamma}(\tau), \tilde{\rho_\gamma}(0)\rangle \mid_{i\omega_m\to\omega+i\delta} \tag{3}$$

with

$$\tilde{\rho_\gamma} = \sum_{\mathbf{k},\sigma}\sum_{n,m} \gamma_{n,m}(\mathbf{k}) c^\dagger_{n,\sigma}(\mathbf{k}) c_{m,\sigma}(\mathbf{k}), \tag{4}$$

where n, m denote band indices. If we consider only low energy response (order of meV), the interband transitions can be neglected and we have the vertex of the form

$$\gamma_n(\mathbf{k}) = \hat{e}^i\hat{e}^s + \frac{1}{m}\sum_{j\neq n} \frac{\langle n,\mathbf{k} \mid \hat{e}^s p \mid j,\mathbf{k}\rangle\langle j,\mathbf{k} \mid \hat{e}^i p \mid n,\mathbf{k}\rangle}{\epsilon_n(\mathbf{k}) - \epsilon_j(\mathbf{k}) + \omega^i} + \frac{\langle n,\mathbf{k} \mid \hat{e}^i p \mid j,\mathbf{k}\rangle\langle j,\mathbf{k} \mid \hat{e}^s p \mid n,\mathbf{k}\rangle}{\epsilon_n(\mathbf{k}) - \epsilon_j(\mathbf{k}) - \omega^s}.$$

Here $\hat{e}^{I,S}$ denote the polarization directions of the incident and scattered light respectively. We evaluate the vertex exactly within the tight binding approximation [15–19] and do not resort to the effective mass approximation - one that is valid only when there is a single (or a few) band(s) crossing the fermi level and all other bands much higher than typical incoming light frequency - which is widely used in Raman calculations. Such an approximation completely fails in the Fe superconductors where the spacing between the bands is comparable to the Raman frequency. The vertex function on the nth band can be broken down into various contributions from the irreps of the point group as

$$\gamma_n(\mathbf{k}) = \sum_\mu \gamma_n^\mu \Phi_n^\mu(\mathbf{k}) \tag{5}$$

where the index μ denotes the contributions from the different point group irreps and the functions $\Phi_n^\mu(\mathbf{k})$ are the corresponding basis functions of the μ'th irrep in the n'th band. Screening by the long range Coulomb interaction can be taken into account [8] by including the couplings of the Raman charge density $\tilde{\rho}$ to the isotropic density ρ fluctuations. The screened response is given by

$$\chi^s_{\rho,\tilde{\rho}}(\omega) = \chi_{\tilde{\rho},\tilde{\rho}}(\omega) - \frac{\chi_{\tilde{\rho},\rho}(\omega)\chi_{\rho,\tilde{\rho}}(\omega)}{\chi_{\rho,\rho}(\omega)} \tag{6}$$

with

$$\chi_{\rho,\tilde{\rho}}(\omega) = \chi_{\tilde{\rho},\rho}(\omega) = \sum_{\mathbf{k}} \gamma_n(\mathbf{k})\lambda_n(\mathbf{k},i\omega) \tag{7}$$

and

$$\chi_{\rho,\rho} = \sum_{\mathbf{k}} \lambda_n(\mathbf{k},i\omega) \tag{8}$$

where $\lambda_n(\mathbf{k},i\omega)$ is the Tsuneto function for the nth band defined by(at $T=0$),

$$\lambda_n(\mathbf{k},i\omega) = \frac{\Delta_n(\mathbf{k})^2}{E_n(\mathbf{k})^2}\left(\frac{1}{2E_n(\mathbf{k})+i\omega} + \frac{1}{2E_n(\mathbf{k})-i\omega}\right) \tag{9}$$

Here $E_n(\mathbf{k})^2 = \epsilon_n(\mathbf{k})^2 + \Delta_n(\mathbf{k})^2$. In Eq. 6, the second term is the contribution from the long range coulomb interaction and the first is the bare Raman response. In the case of two bands, the total response can be written as a sum of screened responses for the individual bands plus a mixing term [8] which vanishes in the special case where the vertices and the gaps are identical for the two bands. The overall Raman response can then be written as

$$Im\chi^{sc}(\omega) = Im\chi_1(\omega) + Im\chi_2(\omega) + Im\Delta\chi(\omega) \tag{10}$$

where

$$\chi_{1,2}(\omega) = \sum_{\mathbf{k}} \gamma^2_{1,2}(\mathbf{k})\lambda_{1,2}(\mathbf{k},i\omega) - \frac{\left(\sum_{\mathbf{k}} \gamma_{1,2}(\mathbf{k})\lambda_{1,2}(\mathbf{k},i\omega)\right)^2}{\sum_{\mathbf{k}} \lambda_{1,2}(\mathbf{k},i\omega)}$$

and

$$\Delta\chi(\omega) = \frac{\sum_{\mathbf{k}}\lambda_1(\mathbf{k},i\omega)\sum_{\mathbf{k}}\lambda_2(\mathbf{k},i\omega)}{\sum_{\mathbf{k}}(\lambda_1(\mathbf{k},i\omega)+\lambda_2(\mathbf{k},i\omega))} \times \left(\frac{\sum_{\mathbf{k}}\gamma_1(\mathbf{k})\lambda_1(\mathbf{k},i\omega)}{\sum_{\mathbf{k}}\lambda_1(\mathbf{k},i\omega)} - \frac{\sum_{\mathbf{k}}\gamma_2(\mathbf{k})\lambda_2(\mathbf{k},i\omega)}{\sum_{\mathbf{k}}\lambda_2(\mathbf{k},i\omega)}\right)^2$$

We will use the expression in Eq.10 to evaluate the response functions in the following derivation.

We make a quick recap of the S_4 symmetric model described by the authors in [6]. Our starting point is the following Hamiltonian similar to [3] on a single copy containing the $x'z$ on the A sublattice and $y'z$ (x' and y'

are along the diagonals to the $Fe-Fe$ bonds) on the B sublattice coupled to each other through the As atoms in between, as

$$H = \sum_{\mathbf{k},\sigma} \psi^{\dagger}_{\mathbf{k},\sigma} \left(\epsilon_+(\mathbf{k}) - \mu)1 + \epsilon_-(\mathbf{k})\tau_3 + \epsilon_{xy}(\mathbf{k})\tau_1\right) \psi_{\mathbf{k},\sigma} \tag{11}$$

with τ_i as the Pauli matrices and $\psi^{\dagger}_{\mathbf{k},\sigma} = (c^{\dagger}_{1,k}, c^{\dagger}_{2,k})$ with $c^{\dagger}_{1,k}$ and $c^{\dagger}_{2,k}$ being the electron creation operators at the sublattice sites A ($x'z$ orbital) and B ($y'z$ orbital) respectively. The band parameters are

$$\begin{aligned}
\epsilon_{\pm}(\mathbf{k}) &= \frac{\epsilon_x(\mathbf{k}) \pm \epsilon_y(\mathbf{k})}{2} \\
\epsilon_x(\mathbf{k}) &= 4t_s cosk_x cosk_y - 4t_d sink_x sink_y \\
&\quad +2t_{3s}(cos2k_x + cos2k_y) \\
&\quad +2t_{3d}(cos2k_x - cos2k_y) \\
\epsilon_y(\mathbf{k}) &= 4t_s cosk_x cosk_y + 4t_d sink_x sink_y \\
&\quad +2t_{3s}(cos2k_x + cos2k_y) \\
&\quad +2t_{3d}(cos2k_x - cos2k_y) \\
\epsilon_{xy}(\mathbf{k}) &= 2t_1(cosk_x + cosk_y)
\end{aligned}$$

with $t_1 = 0.24, t_2 = 0.52, t'_2 = -0.1, t_{s,d} = (t_2 \pm t'_2)/2, t_{3s} = t_{3d} \sim 0, \mu = -0.273$. The matrix elements and electron operators ($d_{1,k}$ and $d_{2,k}$) for the other copy with the $y'z$ orbital on the A and $x'z$ on the B sublattice can be obtained by performing the S_4 symmetry transformation as demonstrated in [6].

We now evaluate and compare the Raman responses for three different cases of the 122-type Iron based superconductors as reported in [13, 14].

Electron overdoped chalcogenide ($Rb_{0.8}Fe_{1.6}Se_2$) : We begin with the simplest case of the electron overdoped Chalcogenides with hole pockets absent from the Γ point. The Fermi surfaces observed in ARPES [20–22] for the electron overdoped chalcogenide consist of two electron pockets at $(\pm\pi, \pm\pi)$ points in the reduced Brillouin zone. Fig 1 (c) shows the plots of the Fermi surfaces seen with different polarization geometries. The values shown near the Fermi surface denote the average value of the square of the Raman vertex in each geometry, on the fermi surface. The A_{1g} case sees an isotropic weight all across the fermi surface whereas the B_{1g} and B_{2g} geometries sample two different regions on the electron pockets (A larger color intensity corresponds to a greater value of the weight. Intensity plots shown are relative and cannot be compared between two geometries). The Raman response for the different polarization geometries is plotted in fig 1 (b). The response in the B_{2g} geometry (with respect to the two atom unit cell) completely dominates when compared to the A_{1g} and B_{1g} cases. This is because of the large weight present on the electron pocket which compensates for its small density of states. The small value of the vertex, in combination with the small density of states present on the electron pocket, leave the responses in the A_{1g} and B_{1g} geometries negligible in comparison with the B_{2g} channel.

FIG. 1. Raman vertices and non-resonant responses for the electron overdoped chalcogenide ($\mu = -0.273, t'_2 = -0.2$ all units in eV). a) Response in the superconducting state as observed in [13]. b) Response evaluated theoretically using the model described in the text. c) Square of the Raman weight factors on the Fermi surface in the three different geometries. We have used a $\Delta_0 cosk_x cosk_y$ form factor for the gap with $\Delta_0 = 0.1$. The laser frequency of $\sim 2.3eV$ corresponding to optical frequencies used in Raman experiments is chosen. The results are robust to changes in the laser frequency as long as it is away from resonance. An impurity broadening of $5meV$ is chosen. The notation of our irreps corresponds to an axis rotated by $\pi/4$ with respect to that used in ref [13].

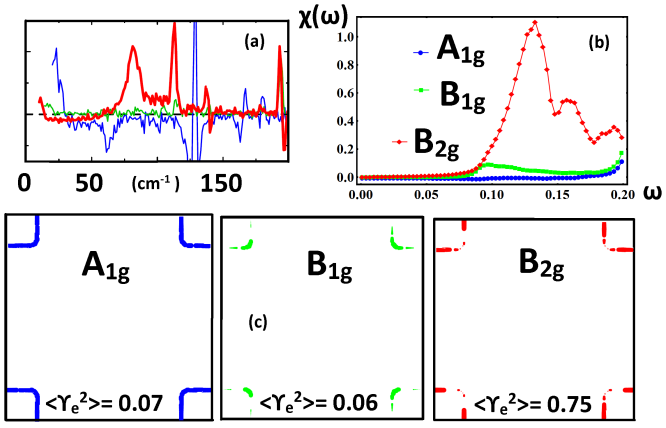

Electron doped pnictide ($Ba(Fe_{1-x}Co_x)_2As_2$): In this case, ARPES [23] sees a small hole pocket centered around the Γ point with the usual two electron pockets at the $(\pm\pi, \pm\pi)$ points in the reduced brillouin zone (See fig 2 (d)). The distribution of the Raman weight on the electron pockets is very similar to that of the electron overdoped chalcogenide discussed previously. However, on the hole pocket, the weight in the A_{1g} geometry is about an order of magnitude larger than that in the other two geometries. This, combined with the large density of states at the hole pocket which is captured in the S_4 model, provides a low intensity broad peak at high energies which consists of contributions from the hole pocket and the mixed response term in eq. 10. The reason for the high intensity peak in the B_{2g} geometry is similar to the previous case because of the large Raman weight on the electron pockets.

Hole doped pnictide($Ba_{0.6}K_{0.4}Fe_2As_2$): Fig 3 shows the Fermi surface, vertex values and the response for the hole doped Iron-pnictides. The experimental fermi surface [24–26] consists of two large hole pockets centered around the Γ point with electron pockets at

FIG. 2. Same as the caption in fig 1 but for the case of electron doped pnictide $Ba(Fe_{1-x}Co_x)_2As_2$, ($\mu = -0.273, t_2' = -0.17$ in eV). The gap on the electron pocket is chosen to be smaller (by $\sim$ 25 percent) than that of the hole pocket consistent with experiment [23]. Data in (a) and (b) taken from [14]. Note that the vertex on the hole pockets in the B_{1g} and B_{2g} geometries is negligible to be seen. The labelling of the irreps is similar to that used in [14].

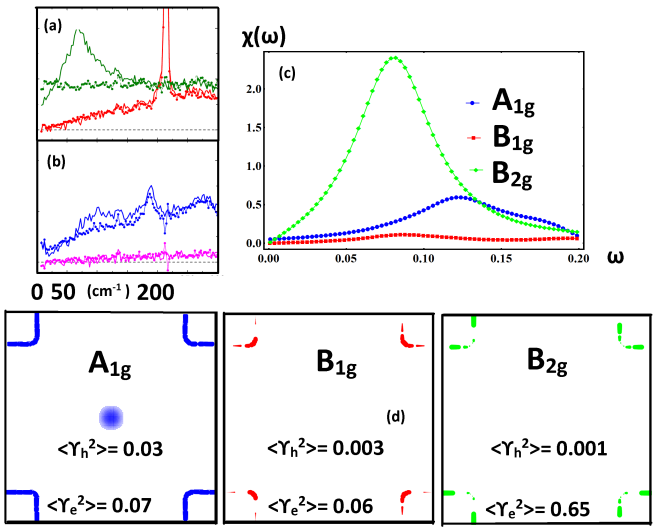

FIG. 3. Same as the caption in fig 1 but for the case of hole doped pnictide $Ba_{0.6}K_{0.4}Fe_2As_2$ ($\mu = -0.21, t_2' = -0.1$ in eV). The gap on the inner hole pocket is chosen to be anisotropic by 10 percent to fit experimental data. The overall intensity in the B_{1g} geometry is multiplied by ≈ 0.8 to match the data. Data in (a) taken from [13]. As before, our irreps are labelled according to an axis rotated by $\pi/4$ with respect to that used in ref [13].

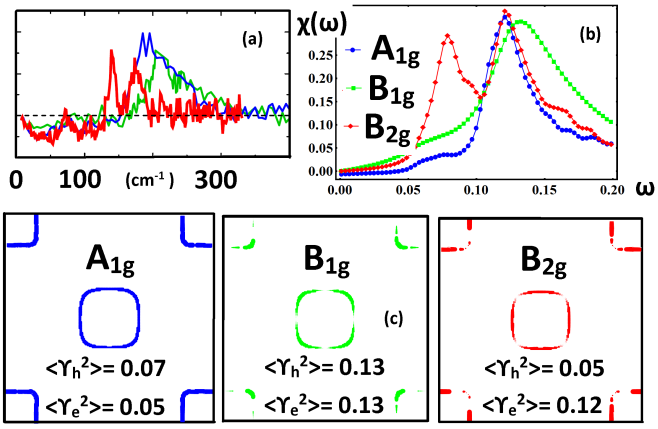

the $(\pm\pi, \pm\pi)$ points in the reduced Brillouin zone. The distribution of the Raman weight is different compared to the previous two cases(fig 3 (c)). In the A_{1g} and B_{1g} geometries, the hole and the electron pockets have comparable weights. However, due to its large density of states, the intensity from the hole pocket completely dominates the spectrum. In contrast, in the B_{2g} case, the hole pocket has a smaller value of the vertex compared to the electron pocket. However, the large density of states compensates for the small value of vertex so that the final response has almost equal contributions from the hole pocket and the electron pocket, giving rise to two distinct peaks at different energies. If, however, according to our picture, the smaller and larger energy peaks in the B_{2g} emerge from the electron and hole pockets respectively, the experimentally observed energy difference between the two shouldn't be more than $\sim 15 - 20 cm^{-1}$. However we see that the energy difference between the two peaks is observed to be $\sim 35 cm^{-1}$ (see for example [27]), a few ten cm^{-1} more. In both B_{2g} and A_{1g} geometries, there are also low energy features (around 80 cm^{-1}) in experimental measurements as shown in Fig3. (a). These features stem from the outer hole pocket that is not present in the S_4 model because the S_4 model only provides two hole pockets rather than three hole pockets at Γ point. Both ARPES [24–26] and Raman [13] have shown a much smaller gap on the outer hole pocket than those on the electron pockets(the ratio between the two gaps is about ~ 0.4). We note that in all above calculations, the gap values that we have chosen for all the three materials is consistent with experiments.

From the above results, we can see that the detailed structure of the Raman vertex and the band curvature are essential in determining the overall intensity of the Raman spectrum. In literature, the Raman vertex is often obtained by using the effective mass approximation; here however, it is determined exactly by taking into account of the non-zero laser frequency. In the case of Iron superconductors, this makes a significant difference - the degeneracy at the M point (in the folded BZ) would have overestimated the vertex and the intensity. Specifically, a naive use of such an approximation would mean that (i) in the Co doped 122 case, the B_{2g} peak would be a lot more exaggerated and (ii) in the hole doped 122 case, the peaks arising from the hole pockets would be heavily overshadowed by the contribution from the electron pockets.

For the electron doped chalcogenide and the electron doped pnictide compounds, our result gives a reasonable quantitative description of the origin of the peaks, their frequencies and intensities, which was only qualitatively argued in refs. [13] and [14]. In the hole doped 122 case, apart from the more quantitative picture, there are several significant qualitative differences in our interpretation of the data. Firstly, in our calculation, the two large peaks observed in the A_{1g} and B_{1g} (2- Fe unit cell notation) in the hole doped 122 compound are from the central hole pocket in contrast to

[13], where the authors argued that the peaks originate from the electron pocket by ruling out the hole pocket as a possible cause (supplemental material from [13]). Their essential argument is that there is an energy difference about ($\sim 15cm^{-1}$) between the peak positions measured in the two cases. However such a small energy difference can be easily explained by the gap variations in the hole pockets[24, 27] instead of ruling out hole pocket contributions. Secondly, our calculation shows that the two large peaks observed in the B_{2g} geometry originate from both electron and hole pockets. The existence of either the Bardasis-Schrieffer [13] or orbital resonance [28] modes suggested in the previous studies, is not necessary. Finally, the previous conclusion in [13] about the existence of the large gap anisotropy on the δ (outer) electron pocket in the hole doped 122 case is not reliable. The conclusion - drawn by observing a combination of the small shoulders close to 80 cm^{-1} (2 Δ_{min}) in the A_{1g} and B_{2g} geometries along with the higher energy peaks close to 200 cm^{-1} (2 Δ_{max}) - is only backed by analogous features seen in a calculation performed in [29]. However, such an interpretation is only valid if the hole pockets do not make a large contribution while our calculation clearly shows that the hole pocket contribution is significant. More importantly, this previous interpretation is incompatible with ARPES results that shows an almost isotropic gap on electron pockets.

In conclusion, we have shown that the two weakly coupled single orbital models proposed in [6] successfully describe the Raman spectra in the superconducting state of the hole doped and electron doped pnictide and chalcogenide superconductors. This is done with a simple $cosk_xcosk_y$ form of the superconducting gap in the Brillouin zone without invoking additional competing forms of the gap.The results are in agreement with the experimental data.

We thank discussion with H. Ding and NN Hao. The work is supported by the Ministry of Science and Technology of China 973 program(2012CB821400), NSFC, and the Strategic Priority Research Program of CAS (Grant No. XDB07000000).

[1] Y. Kamihara, T. Watanabe, M. Hirano, and H. Hosono, Journal of the American Chemical Society **130**, 3296 (2008), ISSN 0002-7863.
[2] D. C. Johnston, Advances in Physics **59**, 803 (2010), ISSN 0001-8732.
[3] S. Raghu, X.-L. Qi, C.-X. Liu, D. Scalapino, and S.-C. Zhang, Physical Review B **77**, 220503 (2008).
[4] P. A. Lee and X.-G. Wen, Physical Review B **78**, 144517 (2008).
[5] K. Kuroki, S. Onari, R. Arita, H. Usui, Y. Tanaka, H. Kontani, and H. Aoki, Physical Review Letters **101**, 087004 (2008).
[6] J. Hu and N. Hao, Physical Review X **2**, 021009 (2012).
[7] T. Devereaux and D. Einzel, Physical Review B **51**, 16336 (1995).
[8] M. Klein and S. Dierker, Physical Review B **29**, 4976 (1984).
[9] T. P. Devereaux and R. Hackl, Reviews of modern physics **79**, 175 (2007).
[10] A. V. Chubukov, I. Eremin, and M. M. Korshunov, Physical Review B **79**, 220501 (2009).
[11] I. Mazin, T. Devereaux, J. Analytis, J.-H. Chu, I. Fisher, B. Muschler, and R. Hackl, Physical Review B **82**, 180502 (2010).
[12] G. Boyd, P. Hirschfeld, and T. Devereaux, Physical Review B **82**, 134506 (2010).
[13] F. Kretzschmar, B. Muschler, T. Bhm, A. Baum, R. Hackl, H.-H. Wen, V. Tsurkan, J. Deisenhofer, and A. Loidl, Physical review letters **110**, 187002 (2013).
[14] B. Muschler, W. Prestel, R. Hackl, T. Devereaux, J. Analytis, J.-H. Chu, and I. Fisher, Physical Review B **80**, 180510 (2009).
[15] L. L. Y. Voon and L. Ram-Mohan, Physical Review B **47**, 15500 (1993).
[16] M. Graf and P. Vogl, Physical Review B **51**, 4940 (1995).
[17] T. G. Pedersen, K. Pedersen, and T. B. Kriestensen, Physical Review B **63**, 201101 (2001).
[18] B. A. Foreman, Physical Review B **66**, 165212 (2002).
[19] M. Cruz, M. Beltrn, C. Wang, J. Tagea-Martnez, and Y. G. Rubo, Physical Review B **59**, 15381 (1999).
[20] X.-P. Wang, T. Qian, P. Richard, P. Zhang, J. Dong, H.-D. Wang, C.-H. Dong, M.-H. Fang, and H. Ding, EPL (Europhysics Letters) **93**, 57001 (2011), ISSN 0295-5075.
[21] D. Mou, S. Liu, X. Jia, J. He, Y. Peng, L. Zhao, L. Yu, G. Liu, S. He, and X. Dong, Physical review letters **106**, 107001 (2011).
[22] L. Zhao, D. Mou, S. Liu, X. Jia, J. He, Y. Peng, L. Yu, X. Liu, G. Liu, and S. He, Physical Review B **83**, 140508 (2011).
[23] K. Terashima, Y. Sekiba, J. Bowen, K. Nakayama, T. Kawahara, T. Sato, P. Richard, Y.-M. Xu, L. Li, and G. Cao, Proceedings of the National Academy of Sciences **106**, 7330 (2009), ISSN 0027-8424.
[24] D. Evtushinsky, D. Inosov, V. Zabolotnyy, A. Koitzsch, M. Knupfer, B. Bchner, M. Viazovska, G. Sun, V. Hinkov, and A. Boris, Physical Review B **79**, 054517 (2009).
[25] H. Ding, P. Richard, K. Nakayama, K. Sugawara, T. Arakane, Y. Sekiba, A. Takayama, S. Souma, T. Sato, and T. Takahashi, EPL (Europhysics Letters) **83**, 47001 (2008), ISSN 0295-5075.
[26] Z. Lin, L. Hai-Yun, Z. Wen-Tao, M. Jian-Qiao, J. Xiao-Wen, L. Guo-Dong, D. Xiao-Li, C. Gen-Fu, L. Jian-Lin, and W. Nan-Lin, Chinese Physics Letters **25**, 4402 (2008), ISSN 0256-307X.
[27] K. Nakayama, T. Sato, P. Richard, Y. M. Xu, Y. Sekiba, S. Souma, G. F. Chen, J. L. Luo, N. L. Wang, H. Ding, et al., EPL (Europhysics Letters) **85**, 67002 (2009), ISSN 0295-5075 1286-4854.
[28] W.-C. Lee and P. W. Phillips, EPL (Europhysics Letters) **103**, 57003 (2013), ISSN 0295-5075.
[29] D. Scalapino and T. Devereaux, Physical Review B **80**, 140512 (2009), ISSN 0163-1829.